Chapter 4 Application of OPLLs in coherent beam combining

4.1 Introduction of coherent beam combining

4.1.1 Spectral beam combining vs coherent beam combining

High power, high brightness lasers with diffraction limited beam quality have been sought since the earliest days of laser technology. Today, high power gas lasers, solid state lasers and fiber lasers are able to output thousands of watts of light under continuous-wave operation. Further increase of the power will be limited by thermo-optic effects, nonlinear effects, and material damage. A promising solution to these challenges is to use beam combining techniques, meaning to combine the outputs of a number of lasers or amplifiers to obtain a single output. The goal of beam combining is not only to scale the power, but also the brightness. For this purpose the beam quality needs to be preserved. Semiconductor lasers and fiber amplifiers have attractive attributes for beam combining because of their ease in building array formats, their high efficiency, and their ability to get near diffraction-limited beams from the individual elements[44-49]. There are generally two classes of beam combining with increased brightness: spectral beam combining (SBC)[44, 49, 50] and coherent beam combining (CBC)[25, 27, 29, 51].

CBC combines an array of element beams with the same frequency and controlled relative phases such that there is constructive interference. This is analogous to phased-array transmitters in the radio-frequency (RF) and microwave portions of the electromagnetic spectrum, but in the optical domain. Beam steering by controlling the relative phase of each element beam is also possible with CBC. However CBC has proven to be difficult because of the shortness of the optical wavelength and the requirement that the phases of the array elements be controlled to a small fraction of a wavelength.

The general principle of SBC is to have several beams with non-overlapping optical spectra and cto ombine them at some kind of wavelength-sensitive beam combiner such as a prism, a diffraction grating, a dichroic mirror, or a volume Bragg grating, which can deflect incident beams according to their wavelengths so that afterwards these all propagate in the same direction. To combine the outputs of a large number of lasers, one requires that each laser must have high wavelength stability and the beam combiner must have sufficient dispersion. Compared with CBC, SBC has the advantage of not requiring the mutual temporal coherence of the combined beams. This eliminates some important technical challenges and makes it much easier to obtain stable operation at high power levels.

4.1.2 Tiled-aperture and filled-aperture CBC

CBC is of interest, however, for applications requiring both high power and narrow spectrum. There are a few excellent reviews of CBC systems[45-48]. Depending on the combining implementation, CBC can be subdivided into tiled-aperture approach (side-by-side combining leading to a larger beam size but reduced divergence), and filled-aperture approach (where several beams are combined to a single beam with the same beam size and divergence, using e.g. beam splitters). The function of beam steering can only be realized with the tiled-aperture approach.

As an example of the side-by-side tiled-aperture combining, consider four beams with top-hat intensity profiles of rectangular cross section and flat phase profiles. One may arrange these profiles to obtain a single beam with two times the dimensions, or four times the area, and of course four times the power. If the beams are all monochromatic and mutually coherent, and the relative phases are properly adjusted to obtain essentially plane wavefronts over the whole cross section, one obtains a beam divergence which is only half that of each single beam. As a result, the beam quality is preserved, and the brightness of the far field can be sixteen times that of each single beam. In practice, the top-hat beam profile is not easily obtainable, and the gaps between the individual beams (i.e., the non-unity fill factor) together lead to side lobes in the far-field beam pattern and reduce the beam quality and brightness.

To understand the principle of the filled-aperture techniques, consider a beam splitter with 50% reflectivity. Overlapping two input beams at this beam splitter will in general lead to two outputs, but one can obtain a single output if the two beams are mutually coherent and adjusted so that there is destructive interference for one of the outputs. This technique makes it easier to preserve the beam quality and does not require special beam shapes, but it may be less convenient for large numbers of emitters, where a series of beam combining stages is required. If any one stage fails, the performance of the whole system degrades significantly.

In any case, the constructive interference plays the key role, and the mutual coherence of the combined beams is essential. Typically the room-mean-square(rms) relative phase deviations must be well below 1 rad[47, 52]. In addition, the mismatches of the amplitudes, polarizations, pointing and alignment of the element beams all contribute to the degradation of the beam combining efficiency and the beam quality, and need to be well managed.

4.1.3 Methods to Obtain Mutual Coherence

There are a variety of techniques to obtain mutual temporal coherence between the element beams, which are briefly summarized in the following:

- The phases of multiple lasers can be synchronized by some kind of optical coupling, such as evanescent wave or leaky-wave coupling[53-56]. This approach has been extensively used, particularly with laser diode arrays [56], where optical coupling can be obtained simply by placing the waveguides sufficiently close together. This may also be applied to multi-core optical fibers. In-phase coupling of the array elements is desired to obtain high on-axis far-field intensity. However, the coupling is often predominantly out-of-phase, giving a power null on-axis. This can be attributed to the modal gain/loss discrimination. The out-of-phase coupling gives a null between the array elements that, compared with the in-phase coupling, leads to less loss if the space between the elements is lossy, and higher gain because of better spatial overlap of the mode with the gain region. Another issue is tolerance the phase error. While scaling to a large array of N elements, the degradation of the on-axis field intensity and beam quality increases with N^2 due to the nature of the correlated phase error between the array elements[52].

- The out-of-phase coupling problem is partially avoided in the common-resonator techniques, where the beams are fully combined at the output coupler, but split within the resonator (laser resonator) to be amplified in different gain elements [57-59]. To force the lowest order transverse-mode operation (corresponding to the in-phase coupling) an intracavity spatial filter can be used to select the mode. Though this approach has been successful at low power, it is difficult to obtain the lowest order transverse mode operation as power increases due to the thermally induced variation in the optical path length.
- Another extensively studied method of obtaining mutually coherent monochromatic beams is to use active-feedback, where the differential phases among the array elements are detected and then feedback is used to equalize the optical path lengths modulo 2π [25, 28, 60, 61]. This approach has been used in master-oscillator power-amplifier (MOPA) architectures, where a single-frequency laser output is split and amplified, e.g., by high power fiber amplifiers, whose outputs are combined. It has also been used in optical injection locking architecture, where the optical power of a master laser is used to injection-lock an array of slave lasers, whose outputs are amplified by fiber amplifiers and then combined. In both cases the key issues are the detection of the differences in optical path length and the design of a phase control servo system

with sufficient bandwidth and dynamic range to correct for these variations. For example, one can adjust the pump power of each amplifier or use an optical phase modulator, a fiber stretcher, or an acoustic optical modulator in front of each amplifier input to adjust the phase of each element beam. The resulting phase-coherent beams can be combined with either the filled-aperture approach or the tiled-aperture approach.

The CBC system I am going to discuss in this thesis falls into the last category, the active feedback control. We propose that mutual coherence between the element beams be established by locking an array of slave lasers to one master laser using OPLLs. Following each slave laser, a fiber amplifier can be used to increase the power. However, the differential phase between the outputs of the fiber amplifiers varies due to optical path length variation in the fiber, which needs to be corrected for. As I have pointed out in Chapter 2, in a heterodyne OPLL, the phase of the slave laser depends on the phase of the RF offset signal. Hence, a RF phase or frequency shifter, instead of an optical phase or frequency shifter, can be used to correct for the optical path length variation. The use of OPLLs thus eliminates the need for expensive and bulky optical phase modulators or acoustic optical modulators, and enables a full electronic phase control servo, which can significantly reduce the cost and size of the CBC system.

In this chapter, I present both the theoretical and the experimental study of the frequency/phase control of the element beams with multilevel OPLLs.

4.2 Synchronizing two SCLs with OPLLs

In Chapter3 I have demonstrated the phase locking of different commercial SCLs, including a 16dBm JDSU DFB laser at 1538nm, a 1W QPC master-oscillator-power -amplifier (MOPA) at 1548nm, and a 18dBm IPS external cavity laser at 1064nm. To demonstrate the idea of CBC with OPLLs, I combined two OPLLs in which the two slave lasers are locked to the same master laser and have the same frequency.

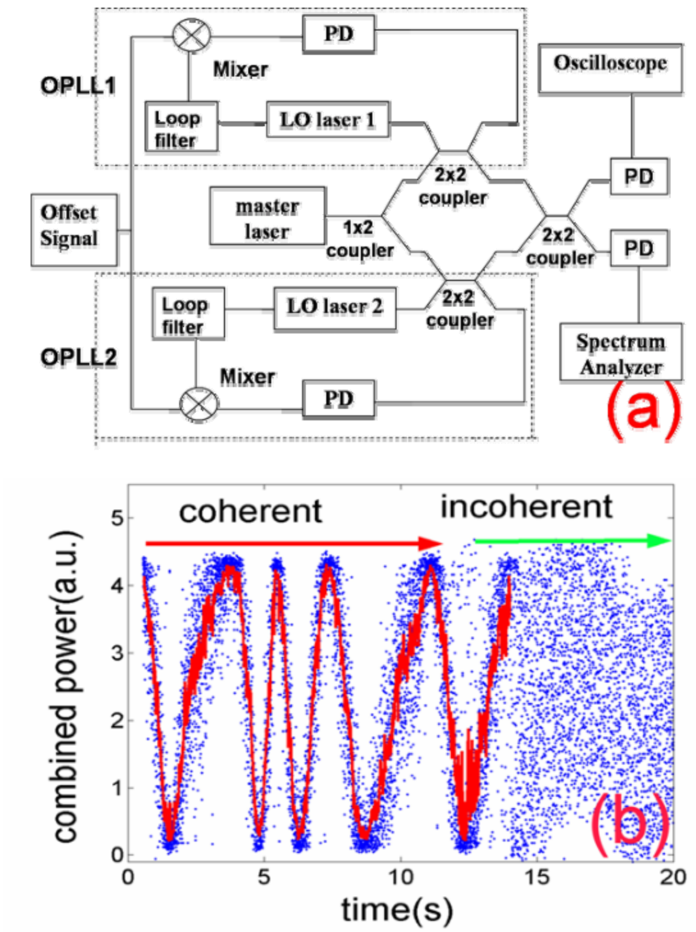

Fig. 4.1 (a) Schematic diagram of coherent beam combining of two SCLs locked to a common master laser. (b) Time domain measurement of the combined power. The blue dots are the measured data, the red solid line is the smoothed data.

Fig. 4.1(a) shows the schematic diagram of combining two OPLLs using the filled-aperture approach. OPLL1 and OPLL2 share the same master laser, which is an Agilent 81640A tunable laser, and the slave lasers are JDSU DFB lasers. The power of the master laser distributed to the OPLLs is typically -3dBm and could be reduced to -15dB since a RF amplifier can be used to compensate for the loop gain. A 1.48GHz RF offset signal provided by the HP 8565E signal generator is split and distributed to both OPLLs. The optical signals of the two slave lasers are combined with a 3dB fiber optical coupler. The locking status of the two OPLLs is monitored in the frequency domain with the HP 8565E spectrum analyzer. The combined signal is detected by a photodetector whose output is displayed in the time domain(Fig. 4.1(b)) using a Tektronix TDS3052B oscilloscope. If one assumes that the amplitudes and the polarization of the two optical signals are matched, the combined power received by the photodetector is

$$P = 2I \cdot \left(1 + \cos\left(\Delta\omega \cdot t + \phi_e\right)\right) \tag{4.1}$$

where I stands for the power of the individual beams, $\Delta\omega$ is the frequency difference, and $\phi_e = \phi_2 - \phi_1$ is the differential phase error between the individual beams. ϕ_2 and ϕ_1 are, respectively, the phases of the signals of slave laser 2 and 1 at the combining point. When at least one of the two slave lasers is not locked to the master laser, the output of the photodetector is an AC signal (the right part of Fig. 4.1(b)) at the frequency $\Delta\omega$. The data appears as a scatter of points, since $\Delta\omega$ is in the MHz range while the time resolution of the oscilloscope is set at 2 seconds. When both the slave lasers are locked ($\Delta\omega = 0$), the individual beams have the same frequency and are coherently added. The output of the photodetector ideally consists of a DC signal which in our case varies slowly on the time scale of seconds as can be seen on the left part of Fig. 4.1(b). This slow variation reflects, as it should, the change of the difference in the optical path lengths experienced by the two individual optical signals due to the slow variation of temperature and environment. The spreading of the coherently combined signal reflects the residual differential phase noise in the OPLLs that I analyzed in Section 2.4. From the degree of scattering of the data I estimate that the rms differential phase error between the two individual signals is about 30 degrees. In Chapter3, based on the measured power spectrum of the locked beat signal, I have calculated that the rms differential phase error between the slave laser and the master laser in a single OPLL is about 19 degrees. Assuming the differential phase errors in two OPLLs are uncorrelated, the rms differential phase error between the two slave lasers should be approximately $\sqrt{2} \times 19 = 27$ degrees. Thus the rms phase error calculated from the frequency domain measurement agrees with that obtained from the time domain measurement.

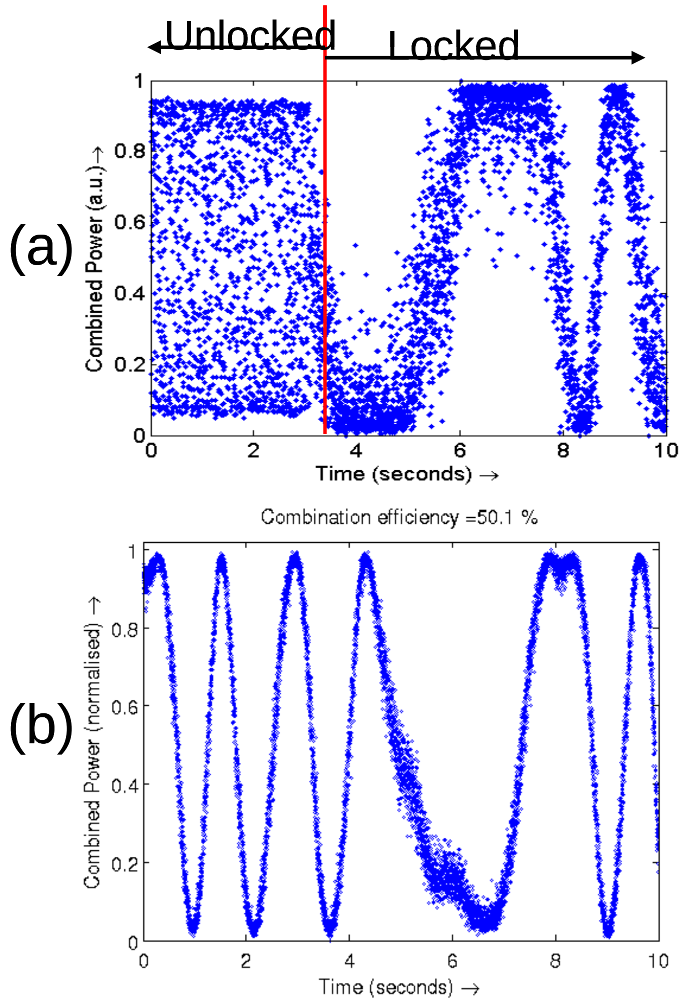

Fig. 4.2 Time domain measurement of the coherently combined power of (a) two QPC MOPAs, (b) two IPS external cavity SCLs

Based on the similar experimental scheme, I repeated the same experiment with the QPC MOPAs and the IPS external cavity SCLs. The Agilent tunable laser is still used as the master laser for the QPC MOPAs. A spectrally stabilized NP Photonics fiber laser with a 3 dB linewidth of 2.5 kHz is used as the master laser for the IPS lasers. The measured combined power in the time domain is shown Fig. 4.2. From the degree of scattering of the data, I estimate that the rms differential phase error between the two individual lasers is about 22 degrees for the QPC MOPAs and 10 degrees for the IPS lasers.

4.3 Correction for the optical path-length variation

Thus far, I have demonstrated the use of OPLLs to synchronize and combine two slave lasers. However one critical issue remains, i.e., the slow variation of the differential phase between the element beams due to the change of the optical path-length in the fibers. A servo system is required to detect this differential phase variation and correct for it. An optical phase shifter (phase modulator or Piezo fiber stretcher) or frequency shifter (an acoustic optical modulator) has previously been used as the phase actuator to correct for the differential phase variation[25, 62]. However these optical phase actuators are typically very expensive (a few thousand dollars each), bulky and can not handle very high optical powers. In the heterodyne OPLLs analyzed in Chapter 2, the phase of the slave laser follows the phase of the RF offset signal within the loop bandwidth. Thus a RF phase shifter can be used to correct for the optical path-length variation.

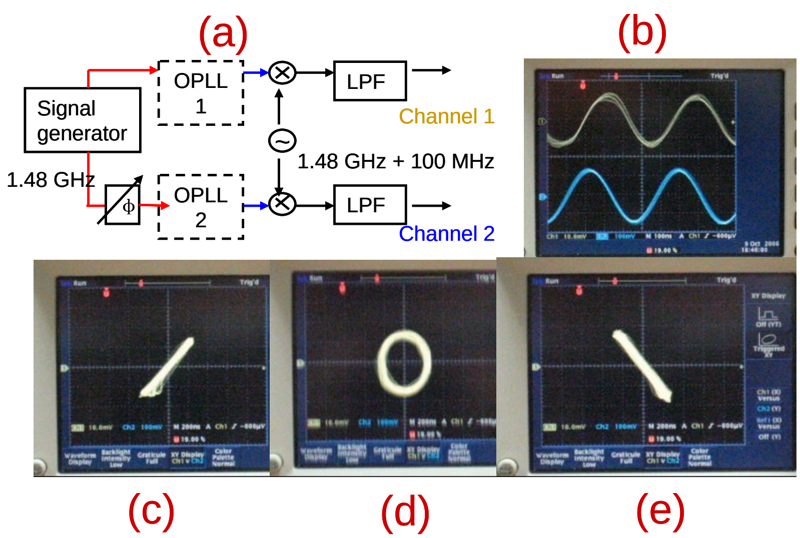

LPF: low pass filter

Fig. 4.3 (a) Schematic diagram of the phase control of the individual MOPA. (b) Comparison of the output waveforms of the two independent OPLLs. (c)-(d) Lissajou curves reflecting the control of the relative phase between the two OPLLs' output signals

4.3.1 Phase control using an RF phase shifter

Fig. 4.3(a) is a schematic diagram depicting the phase control of an individual QPC MOPA using a RF phase shifter. The HP signal generator is still used to provide the RF offset signals (1.48GHz) for the two OPLLs, however the RF signal sent to OPLL2 is now followed by a mechanical RF phase shifter. The beat signals between the master laser and the slave lasers in the two OPLLs are down-converted to 100MHz and the waveforms are compared on the oscilloscope (Fig. 4.3(b)). By adjusting the mechanical RF phase shifter, one can control the relative phase between the beat signals in the two OPLLs, as seen in the Lissajou curves of Fig. 4.3(c)-(e).

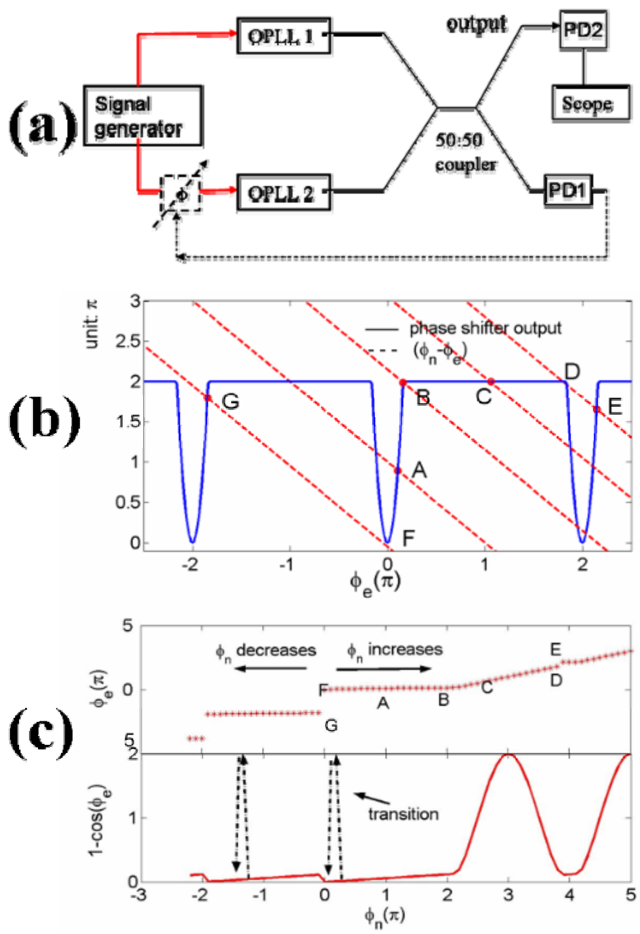

Fig. 4.4(a) Schematic diagram of combining two OPLLs with an additional RF phase shifter loop. (b) Graphic tools to find the steady-state solution of the RF phase shifter

feedback loop. (c) Steady state solution of the differential phase error ϕ_e between the combined individual beams as a function of the phase noise ϕ_n induced by the differential optical path-length variation. The solution depends on both the value and the history of ϕ_n.

Fig. 4.4(a) is a schematic diagram of the combining experiment with a RF phase shifter loop to correct for the optical path-length variation. The details of the OPLLs are given in Fig. 4.1(a) and thus not plotted here. In the filled-aperture scheme the combining element, which is a fiber coupler here, has two outputs. Our goal is to minimize one of the outputs and maximize the other output. The output we want to minimize is detected by a null detector (PD1 in Fig. 4.4(a)), whose output is fed back to the RF phase shifter. Assume the amplitudes, and polarization states of the two individual optical signals are matched, and that their phase difference is $\phi_e(t)$, the output of the null detector is proportional to $1-\cos\phi_e(t)$. Our goal is to maintain $\phi_e(t)$ as close to zero as possible. This signal is amplified and applied to the phase shifter. The resulting phase change of the RF offset signal seen by OPLL2 is

$$f(\phi_e) = G(1-\cos\phi_e), \quad 0 \le f(\phi_e) \le 2\pi \tag{4.2}$$

where G is the phase shifter loop gain, and the phase shifter's dynamic range is from 0 to 2π. Note in Eq. (2.4) of Section 2.2, the phase of the slave laser is inversely related to the phase of the RF offset signal by $\phi_s \sim -\phi_r$. Therefore the phase of the slave laser changes by $-f(\phi_e)$ when the phase of the RF offset signal is changed by $f(\phi_e)$. If the differential optical path-length in the fiber varies by $\phi_n(t)$, the differential phase error between the combined individual beams satisfies

$$\phi_e = \phi_2 - \phi_1 = -f(\phi_e) + \phi_n \tag{4.3}$$

Eq. (4.3) can be solved graphically as illustrated in Fig. 4.4(b). I have assumed that the phase change given by the phase shifter is limited from 0 to 2π and the loop gain is 50. Eq. (4.3) is modified to the form $f(\phi_e) = \phi_n - \phi_e$. The blue solid line in Fig. 4.4(b) represents the RF phase shifter output $f(\phi_e)$, the groups of dashed lines represent $\phi_n - \phi_e$ for different values of ϕ_n. The point of intersection between the blue line and a dashed line satisfies Eq. (4.3) for the particular value of ϕ_n. Two critical issues of this servo system can be deduced from Fig. 4.4(b): First, the limited dynamic range requires a complicated phase unwrapping circuit to control the RF phase shifter once it saturates, e.g., as ϕ_n increases from point F to B, the phase shifter is tracking ϕ_n and ϕ_e is kept small. At the saturation point B, if ϕ_n continues to increase, ϕ_e will increase linearly with ϕ_n and a phase unwrapping circuit is necessary to bring the steady state back to point F. The second issue is that of cycle slips. A small reduction in ϕ_n moves the locking point from point F to G and the loop experiences a cycle slip. In Fig. 4.4(c) I plot the trace of the differential phase error ϕ_e as a function of the fiber path-length variation induced phase noise ϕ_n. If ϕ_n increases monotonously, the phase shifter loop stops tracking after ϕ_n exceeds its dynamic range. If ϕ_n decreases monotonously, frequent cycle slips are expected. A combination of tracking, loss of tracking and cycle slips will be expected in practice, since ϕ_n varies randomly. I performed the CBC experiment with a phase shifter using the IPS lasers, without a phase unwrapping circuit. Fig. 4.5 shows the combined signal measured on the oscilloscope. Comparing this to the result shown in Fig. 4.2(b), one can see that the servo system works only when the phase shifter operates within its dynamic range and is not saturated.

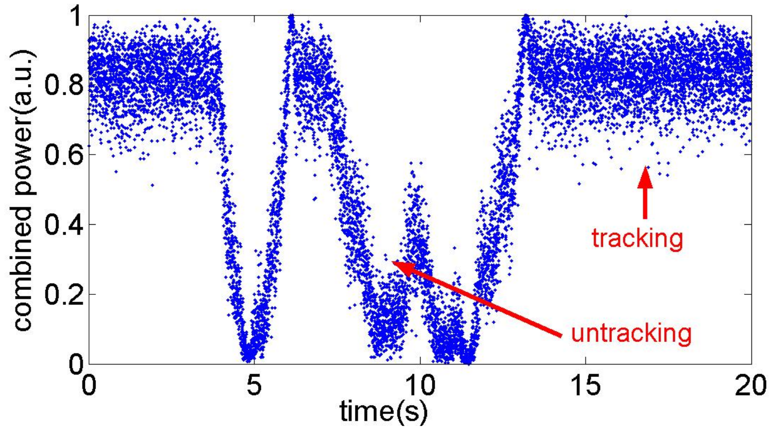

Fig. 4.5 Coherently combined power of two IPS lasers with the servo system made of a RF phase shifter feedback loop without the use of an unwrapping circuit (Fig. 4.4(a))

The issue of the limited dynamic range can be solved by replacing the phase shifter with a frequency shifter, e.g., a voltage-controlled oscillator (VCO), which acts as an integrating phase shifter and has infinite dynamic range.

4.3.2 Phase control using an RF VCO

Fig. 4.6 is a schematic diagram of using a VCO in the servo system. As before, the signal generator provides the RF offset signal for OPLL2. However the RF offset signal of OPLL1 is now provided by a VCO (dashed red line) instead of the signal generator (dashed line (1)). The output of the null detector (PD2) is fed back to the VCO. The VCO feedback loop has two functions. First, it forces the VCO to track the frequency of the signal generator, so that the slave lasers in the two OPLLs have the same frequency. Secondly, it automatically corrects the differential optical path-length variation in the fiber. In this section I analyze this servo system in detail.

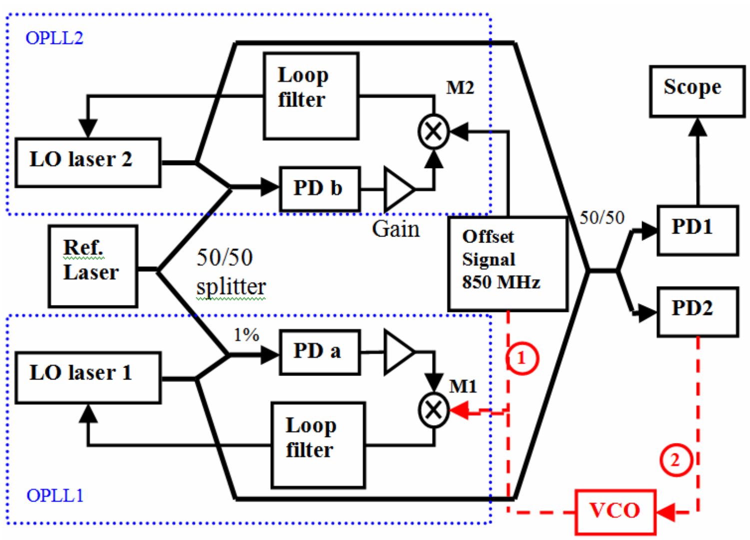

PD: photodetector M: mixer VCO: voltage-controlled-oscillator Scope: oscilloscope

Fig. 4.6 Schematic diagram of combining two OPLLs using a VCO feedback loop to correct for the optical path-length variation

Coupled PLLs picture

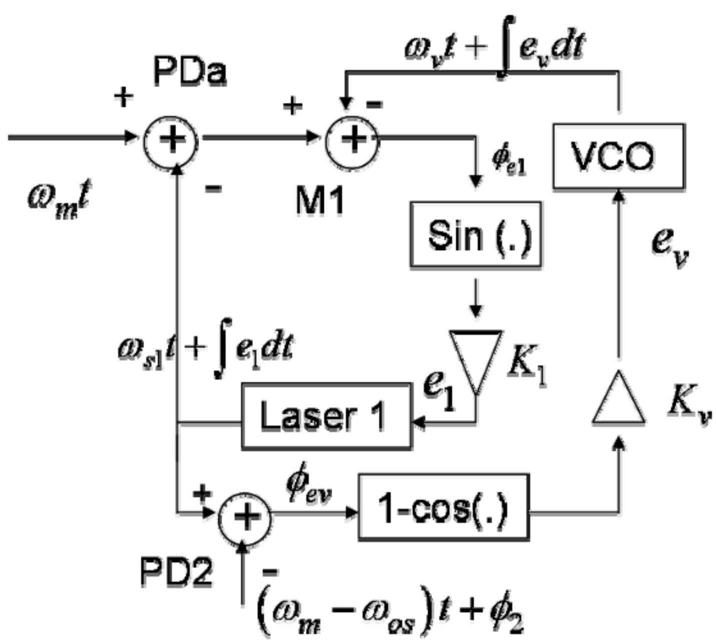

Fig. 4.7 Steady state phase model of the combining system with the VCO loop. The LO laser 2 is locked to the master laser in OPLL2, and is not shown here.

A rigorous analysis of the servo system needs to consider OPLL1 and the VCO loop as a coupled system. The steady state phase model of the VCO combining scheme is shown in Fig. 4.7. The LO laser 2 is locked to the master laser (of frequency ω_m) at a frequency offset of ω_{os}, and has a residual phase noise of $\phi_2(t)$. ω_{s1} and ω_v are the free-running frequencies of the slave laser 1 and the VCO, respectively. K_1 is the OPLL gain given by the product of the gains of the photodetector PDa, mixer, and the loop filter, and the FM responsivity of the laser. Similarly, K_v is the net gain in the VCO branch given by the product of the gains of the photodetector PD2, the FM responsivity of the VCO, and the loop filter. Referring to Fig. 4.7, the differential phase error $\phi_{e1}(t)$ in the OPLL1 and $\phi_{ev}(t)$ in the VCO loop are given by

$$\phi_{e1}(t) = \omega_m t - \underbrace{\left(\omega_{s1} t + \int_{-\infty}^{t} K_1 \sin\phi_{e1}(t) dt \right)}_{\text{phase of slave laser 1}} - \underbrace{\left(\omega_v t + \int_{-\infty}^{t} K_v \left(1 - \cos\phi_{ev}(t)\right) dt \right)}_{\text{phase of the VCO}} \tag{4.4}$$

$$\phi_{ev}(t) = \underbrace{\left(\omega_{s1} t + \int_{-\infty}^{t} K_1 \sin\phi_{e1}(t) dt \right)}_{\text{phase of slave laser 1}} - \underbrace{\left\{ \left(\omega_m - \omega_{os}\right) t + \phi_2 \right\}}_{\text{phase of slave laser 2}} \tag{4.5}$$

Differentiating Eqs. (4.4) and (4.5), one obtains

$$\dot{\phi}_{e1}(t) = \left(\omega_m - \omega_{s1} - \omega_v\right) - K_1 \sin\phi_{e1} - K_v \left(1 - \cos\phi_{ev}\right) \tag{4.6}$$

$$\dot{\phi}_{ev} = \left(\omega_{s1} - \omega_m + \omega_{os}\right) + K_1 \sin\phi_{e1} - \dot{\phi}_2 \tag{4.7}$$

The steady state operating point of the system is obtained by setting the time derivatives of the mixer (M1) and photodetector (PD2) outputs $\phi_{e1}(t)$ and $\phi_{ev}(t)$, to zero in Eqs. (4.6) and (4.7), giving

$$\phi_{e1,ss} = \sin^{-1}\left(\frac{\omega_m - \omega_{s1} - \omega_{os}}{K_1} \right) \tag{4.8}$$

$$\phi_{ev,ss} = \cos^{-1}\left(1 - \frac{\omega_{os} - \omega_v}{K_v}\right) \tag{4.9}$$

The total combined power detected at the photodetector PD1 is

$$P = P_0\left(1 + \cos\phi_{ev}\right) \tag{4.10}$$

where P_0 is the power of one beam. For maximum power combining efficiency (the useful combined output power divided by the input optical power), $\phi_{ev,ss}$ should be as close to zero as possible. Combining Eq. (4.9) and Eq. (4.10), the power combining efficiency can be tuned by varying ω_v, the free-running frequency of the VCO. 100% efficiency is achieved when the VCO free-running frequency is made equal to the offset signal frequency ω_{os}. However, there is a trade-off between the combining efficiency and the frequency of cycle slips, as can be seen from Eq. (4.9). As $\phi_{ev,ss}$ approaches zero, the frequency jitter of the VCO can cause the quantity $\omega_{os} - \omega_v$ to take a negative value, in which case there is no solution to Eq. (4.9) and the VCO loop loses lock. Therefore, the frequency noise of the free-running VCO compared to the loop gain K_v limits the minimum value that $\phi_{ev,ss}$ can take.

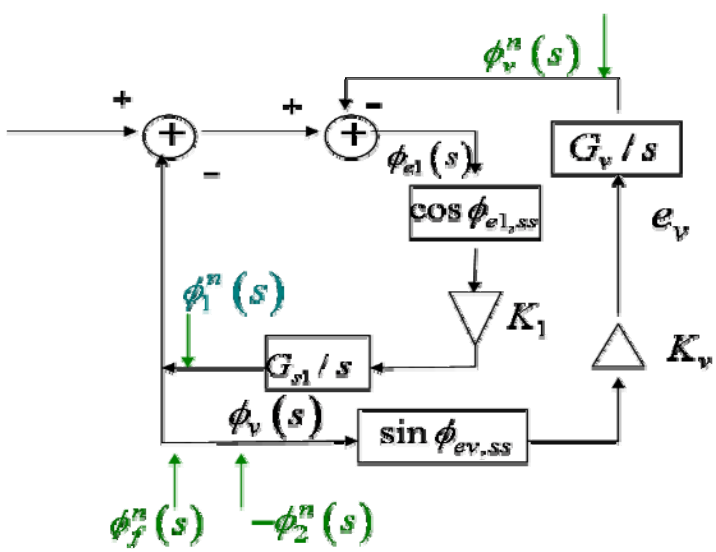

Fig. 4.8 Schematic diagram of the phase noise propagation in the coupled OPLLs

Small signal analysis

Next, I linearise the system about the steady state operating point, in order to analyze its small signal noise property. Strictly speaking, this linearisation is inappropriate because the photodetector output (Eq.(4.10)) is highly nonlinear at the null point. However, a linear analysis is useful in obtaining some physical insight into the problem. The linearised model for the system is shown in Fig. 4.8. One can write down the loop equations

$$\begin{cases} -\left(K_1'\dfrac{\phi_{e1}(s)}{s}+\phi_1^n(s)\right)-\dfrac{K_v'}{s}\phi_{ev}(s)-\phi_v^n(s)=\phi_{e1}(s) \\ K_1'\dfrac{\phi_{e1}(s)}{s}+\phi_1^n(s)+\phi_f^n(s)-\phi_2^n(s)=\phi_{ev}(s) \end{cases} \tag{4.11}$$

where $\phi_1^n(s)$ and $\phi_v^n(s)$ are the intrinsic phase noise of the slave laser 1 and the VCO, $\phi_2^n(s)$ is the phase noise of the locked slave laser 2, and $\phi_f^n(s)$ is the phase noise resulting from the differential optical path-length variation of the combining fibers. K_1' and K_v' are the small signal "loop gains" defined as

$$\begin{cases} K_1' \triangleq K_1\cos\phi_{e1,ss} \\ K_v' \triangleq K_v\sin\phi_{ev,ss} \end{cases} \tag{4.12}$$

where $\phi_{e1,ss}$ and $\phi_{ev,ss}$ are given in Eqs. (4.8) and (4.9). After some algebra, one can simplify Eq. (4.11) to obtain

$$\begin{cases} \phi_{e1}(s)=\dfrac{-\phi_1^n(s)\left(1+K_v'/s\right)+\left(\phi_2^n(s)-\phi_f^n(s)\right)K_v'/s-\phi_v^n(s)}{1+K_1'/s+K_1'K_v'/s^2} \\ \phi_{ev}(s)=\dfrac{\phi_1^n(s)-\left(\phi_2^n(s)-\phi_f^n(s)\right)\left(1+K_1'/s\right)-\phi_v^n(s)K_1'/s}{1+K_1'/s+K_1'K_v'/s^2} \end{cases} \tag{4.13}$$

In principle Eq. (4.13) should be used to analyze the residual phase noise and the performance of the OPLL and the VCO loop. This picture is very complicated and does not provide an intuitive understanding of the servo system. In the next part I will use a simplified picture to analyze the servo system to gain a better intuitive understanding.

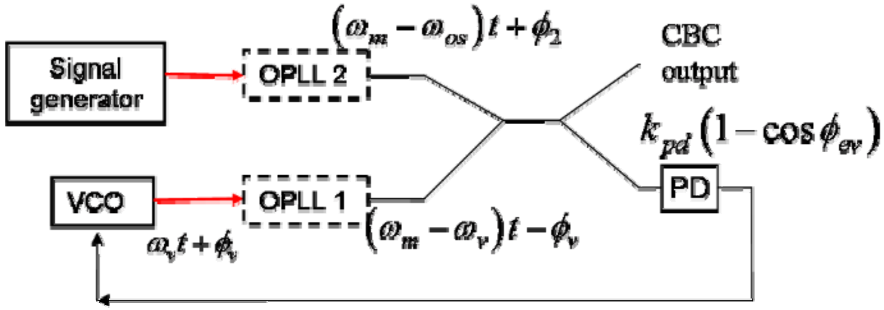

Fig. 4.9 Simplified picture of the VCO servo system.

A simplified picture— the decoupled PLLs

To obtain an intuitive picture of the function of the servo system using the VCO loop, one can simplify the analysis by decoupling OPLL1 and the VCO loop and studying them separately. This simplified picture is illustrated in Fig. 4.9. The validity of this picture can be justified using the following argument: OPLL1, which locks the slave laser 1 to the master laser, typically has a bandwidth of ~10MHz. The VCO loop is used to correct the phase variation in fiber (~Hz) and can be much slower compared to OPLL1. Actually the VCO loop delay, mainly the length of fiber in the fiber amplifier is more than 30m. This long delay, combined with the phase delay of the other electronics, limits the bandwidth of the VCO loop to a few hundred kHz. Thus one can assume that OPLL1 always tracks the phase of the VCO instantly when the phase of the VCO is adjusted to correct for the optical path length variation. Thus the two loops can be studied separately. The analysis of OPLL1 is already given in Chapter 2. In Fig. 4.9, one observes that the VCO loop is similar to a standard PLL, except that the output of the phase detector is proportional to $(1-\cos\phi_{ev})$ instead of $\sin\phi_{ev}$. Following the standard PLL analysis[1], the evolution equation of the VCO loop is

$$\underbrace{\omega_m t - \omega_{v,f} t - K_v \int (1-\cos\phi_{ev}) dt}_{\text{phase of beam 1}} - \underbrace{\left[(\omega_m - \omega_{os})t + \phi_2\right]}_{\text{phase of beam 2}} = \phi_{ev} \tag{4.14}$$

where $\omega_m, \omega_{os}, \omega_{v,f}$ are, respectively, the frequency of the master laser, the RF offset signal, and the free-running VCO, K_v is the VCO loop gain, ϕ_{ev} is the phase difference between the two individual beams at the combining point, and ϕ_2 is the phase of beam 2. In obtaining Eq. (4.14) I have used the equality $\phi_v = K_v \int (1-\cos\phi_{ev}) dt$. Differentiating Eq. (4.14) and setting the time derivatives of ϕ_2 and ϕ_{ev} to zero, one finds the steady state phase error:

$$\phi_{ev,ss} = \cos^{-1}\left(1 - \frac{\omega_{os} - \omega_{v,f}}{K_v}\right) \tag{4.15}$$

So the steady state solution obtained in this decoupled picture is the same as the one obtained in the coupled loops picture (Eq. (4.9)). As long as $0 < (\omega_{os} - \omega_{v,f}) / K_v < 2$, Eq. (4.15) has a solution and the VCO frequency can be locked to the frequency of the offset signal. It is important to note that the steady state phase error under lock, $\phi_{ev,ss}$, which controls the CBC efficiency, can be adjusted by tuning the frequency difference $\omega_{os} - \omega_{v,f}$. High combining efficiency is achieved by minimizing $\phi_{ev,ss}$. However, this comes at the cost of increased cycle-slips caused by the residual phase noise in the OPLLs and frequency jitter of the VCO. The smallest feasible $\phi_{ev,ss}$ is mainly limited by the intrinsic frequency jitter of the free-running VCO and the equivalent frequency jitter of the phase noise in fiber compared to the loop gain K_v. Generally a clean VCO will be helpful in reducing $\phi_{ev,ss}$ and increasing the CBC efficiency. The CBC efficiency can also be increased by increasing the loop gain K_v. However, as I have pointed out, the loop gain of the VCO loop is limited by the long fiber delay if a fiber amplifier is to be used. This dilemma is very similar to the situation I analyzed in Section 3.3.2, where the OPLL bandwidth is limited by the thermal crossover of the FM response and is not enough to hold the loop in lock due to the frequency jitter of SCLs. If the frequency jitter of the VCO is much slower than the bandwidth of the VCO loop, I can use similar strategies to those given in Section 3.3.2, i.e. the use of a lag-lead filter to increase the loop gain at low frequency and reduce $\phi_{ev,ss}$ to a smaller number.

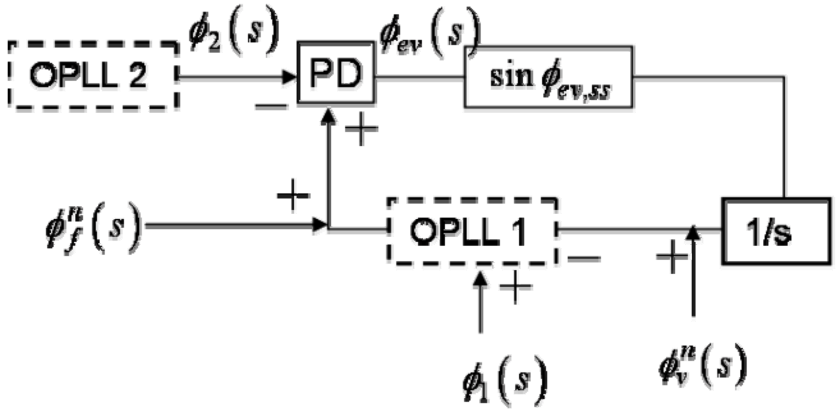

Fig. 4.10 Linearized model of the VCO loop

Next I linearize the system about the steady state point and perform the small signal analysis. A small signal linearized model is presented in Fig. 4.10. $\phi_f^n(s)$ and $\phi_v^n(s)$ are the optical path length variation in fiber and the phase noise of the free-running VCO respectively. ϕ_1 and ϕ_2 denote the residual phase noise of OPLL1 and OPLL2 respectively. Following the standard PLL analysis, one obtains

$$\phi_f^n(s)+\phi_1(s)-\left[\frac{K_v \sin\phi_{ev,ss}}{s}\cdot\phi_{ev}(s)+\phi_v^n(s)\right]-\phi_2(s)=\phi_{ev}(s) \tag{4.16}$$

Solving for $\phi_{ev}(s)$ gives

$$\phi_{ev}(s)=\frac{\phi_1(s)+\phi_f^n(s)-\phi_v^n(s)-\phi_2(s)}{1+\dfrac{K_v \sin\phi_{ev,ss}}{s}} \tag{4.17}$$

In Eq. (4.17) one first observes that a nonzero $\phi_{ev,ss}$ is needed to provide a non-zero small signal loop gain. Secondly, the residual phase noises from OPLL1 and OPLL2 are mostly concentrated at frequencies of a few MHz as I have shown in Chapter 3. Since the bandwidth of the VCO loop is ≤ 100kHz, the VCO feedback loop does not greatly affect the residual phase noise of the OPLLs. A typical high quality VCO possesses very low phase noise compared to a SCL. The optical path length variation $\phi_f^n(s)$ is at very low frequency, according to our experimental observation (~Hz). These noises can be significantly suppressed by the VCO loop with a bandwidth of ~100kHz.

Experimental result

I performed the CBC experiment with the IPS lasers as shown in Fig. 4.6. A MinCircuits ZX95-2150 VCO is used in the experiment. Fig. 4.11(b) shows the combined power using the VCO feedback scheme, and demonstrates the high combining efficiency achieved. Compared with Fig. 4.2(b), the combined power is held at constant with a power combining efficiency of about 94%. The loss of the combining efficiency (6%) can be attributed to the residual differential phase noise in the individual OPLLs, the frequency jitter of the VCO, and the nonzero steady state phase error in the VCO control loop. Mathematically the combining efficiency is expressed as

$$\eta = \left(1 + \overline{\cos\left(\phi_{ev,ss} + \Delta\phi_{ev} + \phi_2 - \phi_1\right)}\right) / 2 \tag{4.18}$$

where $\phi_{ev,ss}$ is the steady state phase error in the VCO loop, $\Delta\phi_{ev}$ is the phase jitter caused by the frequency jitter of the VCO, and ϕ_1 and ϕ_2 are the residual phase noises in OPLL1 and OPLL2 respectively. Assuming $\phi_{ev,ss}$, $\Delta\phi_{ev}$, ϕ_1, and ϕ_2 are small numbers and not correlated, and that $\Delta\phi_{ev}$, ϕ_1, ϕ_2 all have zero means, one can expand Eq. (4.18) and reduce it to

$$\eta \approx 1 - \left(\phi_{ev,ss}^2 + \overline{\Delta\phi_{ev}^2} + \overline{\phi_2^2} + \overline{\phi_1^2}\right) / 4 \tag{4.19}$$

$\overline{\phi_1^2}$ and $\overline{\phi_2^2}$ can be calculated from the measured power spectrum of the locked beat signal (Section 3.2.1), i.e. $\overline{\phi_n^2} = P_n / P_s$. Where P_s is the power of the central carrier signal and P_n is the power of the phase noise and can be obtained by integrating the double-sided power spectral density excluding the central carrier. Fig. 4.11(a) shows a typical power spectrum of the locked beat signal in an IPS laser OPLL. Based on the measured spectrum, the typical values of $\overline{\phi_2^2}$ and $\overline{\phi_1^2}$ are 0.02~0.05. Substituting the numbers in Eq. (4.19), I estimate 1~2% of the combined power is lost due to the residual phase noise in the OPLLs. Another 4% is lost due to the non-zero steady state value $\phi_{ev,ss}$ and the frequency jitter of the VCO. In Fig. 4.11(b), one observes that the mean value of the combined signal slowly increases with time and more cycle slips are seen. This can be attributed to the slow drift of the VCO frequency which reduces $\phi_{ev,ss}$ and leads to more frequent cycle slips.

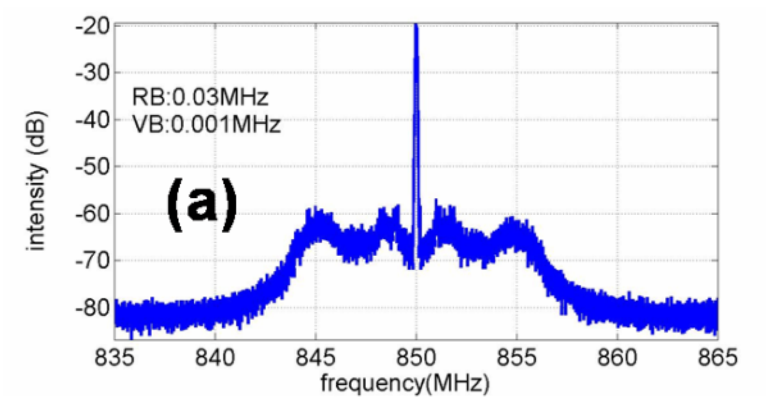

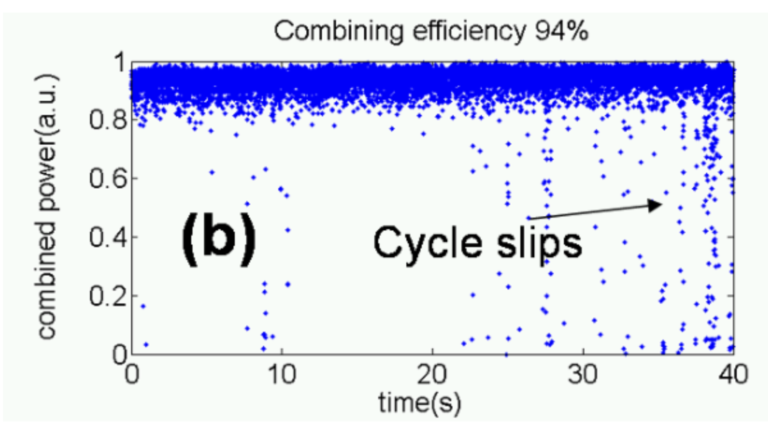

Fig. 4.11 (a) A typical power spectrum of the locked beat signal in an IPS laser OPLL. (b) Measured combined signal of two IPS lasers. The differential optical path-length variation in the fiber is corrected for by the VCO loop.

In conclusion, I have demonstrated the coherent power combining of two commercial SCLs in fiber with the filed-aperture approach using the OPLLs. An additional feedback loop with a VCO has been used to compensate for fluctuations of the differential optical path lengths of the combining optical waves. This full electronic servo scheme eliminates the need for optical feedback or expensive optical components such as optical phase/frequency modulators[3, 4]. However, as I have pointed out in this chapter, that the combining efficiency is reduced by various factors, such as the residual phase noise of the OPLLs and the non-zero steady-state operating point of the VCO loop. It is not clear to what extent these factors will affect the CBC system when this technology is scaled to the combination of a large number of beams. This will be the topic of study in the next chapter.